

Parity-dependent proximity effect in superconductor/antiferromagnet heterostructures

J. W. A. Robinson, Gábor Halász, and M. G. Blamire

Department of Material Science, University of Cambridge, Pembroke Street, Cambridge CB2 3QZ, UK

(Dated: November 17, 2018)

We report the effect on the superconducting transition temperature (T_c) of a Nb film proximity coupled to the synthetic antiferromagnet $\text{Fe}/\{\text{Cr}/\text{Fe}\}_{N-1}$. We find that there is a parity dependence of T_c on the total number of Fe layers, N ; locally T_c is always a maximum when N is even, and a minimum when N is odd. The Fe electron mean free path and coherence length are indicative of dirty limit behavior; as such, we numerically model our data using the linearized Usadel equations with good correlation.

PACS numbers: 74.45.+c, 74.62.-c, 74.78.Db

During the past fifteen years the coupling of thin film superconductors (S) to ferromagnets (FM) [1] has been extensively studied. In the most simplistic sense, these electron coupling phenomena can be considered to be mutually exclusive with spin alignment enforced by ferromagnetic exchange and anti-parallel spin alignment necessary for singlet BCS superconductivity. According to theory, the penetration depth of the superconducting proximity effect (SPE) into normal metals (NM) is governed by the electron phase breaking length. When NM is substituted with a FM, the singlet superconducting correlations and phase coherent effects are destroyed by the exchange interaction I within the FM coherence length $\xi_f \propto \sqrt{I}$ because of the splitting of spin-up and spin-down conduction bands. For S/FM bilayers, a consequence of I on S is the non-monotonic dependence of T_c on FM layer thickness (d_f) for when the superconductor is thinner than its BCS coherence length [2]. This can be understood in terms of an interference effect between the transmitted singlet pair wave function through the S/FM interface with the wave reflected at the opposite FM interface.

Recently, Andersen *et al.* [3] predicted a SPE dependence on the number of antiferromagnetic (AF) atomic planes (N) in S/AF/S junctions such that the junction's ground state is 0 or π depending on whether N is even or odd. Experimentally, this SPE dependence on N is difficult to realize because it demands atomic thickness control of the AF. So far, experiments looking at the proximity of S to AFs have focused on thicker AF layers [4] where this parity dependence does not exist. A way to investigate a parity dependent SPE is to use synthetic antiferromagnets (SAFs) which exploit the AF coupling of FM layers separated by a NM spacer [5].

So far, the proximity effect of SAFs coupled to S materials have not been considered although the T_c dependence of complicated multilayers have been extensively studied [6]; for example, the control of T_c in pseudo-spin valve FM/S/FM structures has been proposed [7] and realized experimentally [8] with mK differences in T_c between parallel (P) and anti-parallel (AP) FM configurations. The most similar structure to the one we study here was proposed by Oh *et al.* [9] in which the S layer is in proximity to decoupled FM/NM/FM. In this Letter, we report the proximity-suppression of T_c of a Nb film coupled to a $\text{Fe}/\{\text{Cr}/\text{Fe}\}_{N-1}$ SAF. In doing this, we find that T_c has a pronounced parity dependence on N such

that when N is even, T_c is a local maximum and, conversely, when N is odd, T_c is a local minimum.

Films were grown in Ar (1.5 Pa) on oxidized (120 nm) Si (100) (surface area: $5\text{-}10 \times 5 \text{ mm}^2$) in a diffusion-pumped ultrahigh vacuum sputter deposition system, consisting of the following: three dc magnetrons; a computer operated (rotating) sample table; a liquid N_2 cooling jacket; and a residual gas analyzer. The vacuum system was baked-out overnight prior to each experiment, reaching a base pressure of $1\text{-}4 \times 10^{-6}$ Pa. One hour before depositing, the system was cooled with liquid N_2 giving a final base pressure of $1\text{-}3 \times 10^{-8}$ Pa, a residual O_2 pressure of $\leq 4 \times 10^{-9}$ Pa, and an outgassing rate of $\approx 1 \times 10^{-8} \text{ Pa s}^{-1}$. Targets (Nb, Fe, and Cr of 99.9% purity), were pre-sputtered for ~ 15 minutes to remove contaminants from their surfaces and to further reduce the base pressure of the vacuum chamber by getter sputtering. To control film thickness (d) and to ensure clean interfaces, films were grown in a single sweep by rotating the substrates around the symmetry of the chamber under stationary targets. Growth rates were pre-calibrated by growing films on patterned substrates and, from a lift-off step-edge, d for each material was established using an atomic force microscope. Typical growth rates with a sweep speed of 1 rpm per pass were: 1.0 nm for Cr; 0.6 nm for Fe; and 1.4 nm for Nb. The average film roughness was $\leq 3 \text{ \AA}$ over $1 \text{ }\mu\text{m}$.

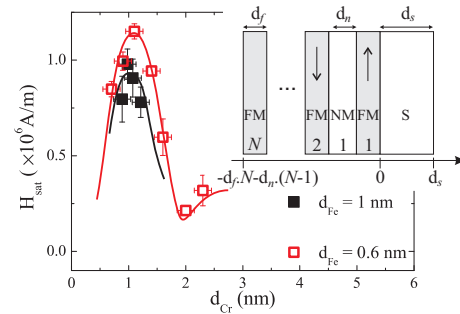


FIG. 1: (color online). Dependence of H_{sat} on d_{Cr} in $\text{Nb}(20\text{nm})/\text{Fe}/\{\text{Cr}/\text{Fe}\}_{\times 7}$ films for: $d_{Fe}=0.6 \text{ nm}$ (\square); and $d_{Fe}=1.0 \text{ nm}$ (\blacksquare). Solid lines are to guide the eye. Inset: illustration of $\text{S}/\text{FM}/\{\text{NM}/\text{FM}\}_{N-1}$ structure with N FM layers and $N-1$ NM layers. Vertical arrows indicate FM polarization direction.

The antiferromagnetic interlayer exchange coupling (AFC) between the Fe layers was investigated in two sets of Nb/Fe/{Cr/Fe}₇ films: for $d_{Fe}=0.6$ nm; and for $d_{Fe}=1.0$ nm. d_{Nb} was constant (20 ± 1 nm) while d_{Cr} varied in the 0.5-2.5 nm range. A 2.8 nm capping layer of Nb was grown on the top Fe layer. To quantify AFC in these films and to optimize d_{Cr} to give the largest AFC energy J (given by $-4J = \mu_0 H_{sat} M d_{Fe}$ where M is the magnetization of the Fe), the required saturating field H_{sat} needed to align the Fe layers was measured with a vibrating sample magnetometer at room temperature as a function of d_{Cr} ; see Fig.1. For $d_{Fe} = 0.6$ nm, H_{sat} is a maximum value of $(1.16 \pm 0.04) \times 10^6$ A/m for $d_{Cr} = 1.0 \pm 0.2$ nm with $M \approx 0.8 \times 10^6$ A/m (similar to [10]). This corresponds to $-J \approx 1.8 \times 10^{-4}$ Jm⁻², which compares well to previously reported energies [5]. To achieve the most efficient AFC, we chose $d_{Fe} = 0.6$ nm and $d_{Cr} = 0.9$ nm for the appropriate layer thicknesses.

To establish a d_{Nb} range that is strongly affected by the presence of the SAF film, the T_c of both bare Nb and Nb/Fe/{Cr/Fe}₇ films was measured in the 15-45 nm range; see Fig. 2. The critical d_{Nb} is ≈ 12 nm. T_c was estimated by measuring the resistance of a film as a function of temperature ($R(T)$) using a standard four contact technique; for this, two instruments were used: a custom made liquid He dip probe and a pumped He-4 temperature insert. To make electrical contacts, films were ultrasonically wire-bonded onto copper carriers with Al wire (25 μ m diameter). Samples were fixed to their carriers with silver conducting paint. An ac current of $\pm 10 \mu$ A was applied. T_c was estimated from warming curve data and defined as the mid-point of the $R(T)$ transition.

Fig. 3 shows the dependence of T_c on N for two Nb thicknesses: (a) 22 nm and (b) 18 nm. We see that T_c is a local maximum when N is even and vice-versa. The magnitude of $|T_c(N+1) - T_c(N)|$ decreases as N increases: the largest for $T_c(2) - T_c(3) = 1.38$ K in (a) and 2.06 K in (b). Assuming dirty limit behaviour in the multilayers ($\xi > \ell$), we have adapted the Usadel equations, as discussed by Fominov *et al.* [11] and Oh *et al.* [9], to model the situation; as illustrated in the inset of Fig. 1.

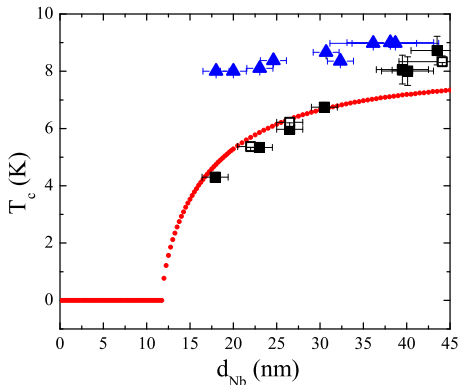


FIG. 2: (color online). Dependence of T_c on d_{Nb} : bare Nb (\blacktriangle); two Nb/Fe/{Cr/Fe}₇ sets for $d_{Fe} = 0.6$ nm and $d_{Cr} = 0.9$ nm (\square and \blacksquare); theory fit (\bullet) explained in text.

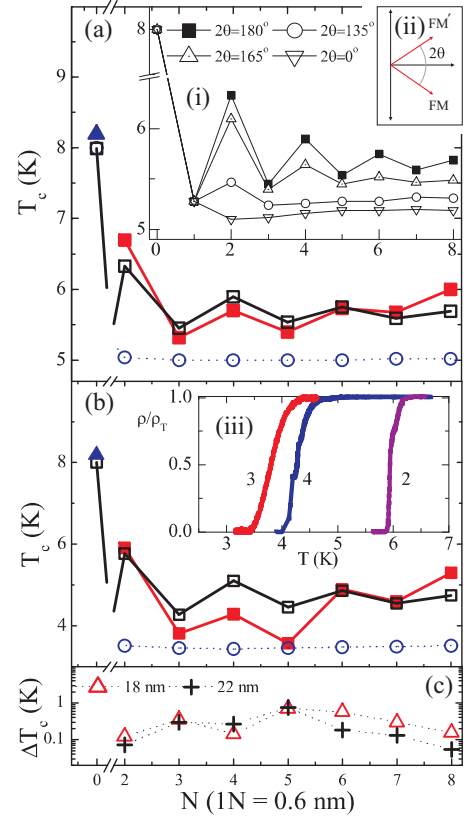


FIG. 3: (color online). Experimental (\blacksquare) and theoretical (\square) dependence of T_c on N : (a) $d_{Nb} = 22$ nm; (b) $d_{Nb} = 18$ nm. For comparison, data points (\odot) are for a theoretical S/FM bilayer and (\blacktriangle) for bare Nb taken from Fig. 2. Inset: (i) the theoretical non-collinear case for various 2θ angles between FM layers; (ii) illustration defining 2θ between two FM layers; (iii) typical resistivity curves for $N = 2, 3$ and 4 in the function of T . (c) Spread in T_c (ΔT_c) defined as 20%-80% of the transition.

The normal Green function is $G = \text{sgn}(\omega_l)$ when $T \approx T_c$ and the linearized Usadel equations for the anomalous Green function F are:

$$\frac{\hbar D_s}{2} \frac{d^2 F_s}{dx^2} - \hbar |\omega_l| F_s + \Delta = 0 \quad (1)$$

inside the S layer,

$$\frac{\hbar D_f}{2} \frac{d^2 F_{fk}}{dx^2} - \hbar |\omega_l| F_{fk} - i(-1)^k I \text{sgn}(\omega_l) F_{fk} = 0 \quad (2)$$

inside the k th ($k = 1, 2, \dots, N$) FM layer and

$$\frac{\hbar D_n}{2} \frac{d^2 F_{nk}}{dx^2} - \hbar |\omega_l| F_{nk} = 0 \quad (3)$$

inside the k th ($k = 1, 2, \dots, N-1$) NM layer.

The appropriate diffusivities are D_s , D_f and D_n , while Δ is the superconducting pairing potential in the S layer. The $(-1)^k$ factor before I accounts for the alternating polarization of the FM layers. The Usadel equations are supplemented by the self-consistency equation

$$\Delta \ln \left(\frac{T_0}{T} \right) = \pi k_B T \sum_{\omega_l} \left(\frac{\Delta}{\hbar |\omega_l|} - F_s \right), \quad (4)$$

where the summation goes over the Matsubara frequencies $\omega_l = (2l + 1)\pi k_B T / \hbar$ with all integers l . T_0 is the T_c of bare S of thickness d_s , i.e. see Fig.2. The anomalous function F obeys the boundary conditions

$$\sigma_a \frac{dF_a(x_{a,b})}{dx} = \sigma_b \frac{dF_b(x_{a,b})}{dx} = \frac{F_b(x_{a,b}) - F_a(x_{a,b})}{R_{a,b}} \quad (5)$$

at the points $x = x_{a,b}$ separating any a and b layers; a and b can be either of the S, FM or NM layers and in each case we use the appropriate normal-state conductivities (σ_a and σ_b) as well as the appropriate interfacial resistance per unit area $R_{a,b}$ between a and b layers. Since all the FM and NM layers are identical, the three conductivities are σ_s , σ_f and σ_n and the two interfacial resistances are $R_{s,f}$ and $R_{f,n}$.

If we introduce the formal vector $\Phi_b = (F_b, dF_b/dx)$, we can turn Eq. (2) and (3) into vector equations for Φ_b (b refers to an arbitrary layer again), which take the common form

$$\frac{d}{dx} \Phi_b = \mathbf{M}_b \Phi_b \quad \text{with} \quad \mathbf{M}_b = \begin{pmatrix} 0 & 1 \\ k_b^2 & 0 \end{pmatrix}, \quad (6)$$

where the values of k_b^2 are

$$k_{fk}^2 = \frac{2\hbar|\omega_l| + 2i(-1)^k I \text{sgn}(\omega_l)}{\hbar D_f} \quad \text{and} \quad k_{nk}^2 = \frac{2|\omega_l|}{D_n} \quad (7)$$

in the k th FM and the k th NM layers, respectively. Eq. (6) is a simple linear differential equation. If Φ_b is known at the left side ($x = x_{a,b}$) of a layer, its value at the right side ($x = x_{a,b} + d_b$) can be expressed in terms of matrix exponentials

$$\Phi_b(x_{a,b} + d_b) = \mathbf{A}_b \Phi_b(x_{a,b}) \quad \text{with} \quad \mathbf{A}_b = \exp(\mathbf{M}_b d_b). \quad (8)$$

The boundary conditions (Eq. 5) between any two layers a and b can be written in the vector form as

$$\Phi_b(x_{a,b}) = \mathbf{B}_{b,a} \Phi_a(x_{a,b}) \quad \text{with} \quad \mathbf{B}_{b,a} = \begin{pmatrix} 1 & R_{a,b}\sigma_a \\ 0 & \sigma_a/\sigma_b \end{pmatrix}. \quad (9)$$

The derivative of the anomalous function F vanishes at the left end of the multilayer, therefore $\Phi_{fN}(-d_f N - d_n(N-1)) = (C, 0)$, where C is a complex number. The formal vector Φ at the left side of the S layer is now expressed in the function of C by systematically going through the layers and using the appropriate matrices appearing in Eqs. (8) and (9):

$$\Phi_s(0) = \mathbf{L}(\omega_l) \begin{pmatrix} C \\ 0 \end{pmatrix}, \quad \text{where} \quad (10)$$

$$\mathbf{L}(\omega_l) = \mathbf{B}_{s,f1} \prod_{k=1}^{N-1} [\mathbf{A}_{fk} \mathbf{B}_{fk,nk} \mathbf{A}_{nk} \mathbf{B}_{nk,f(k+1)}] \mathbf{A}_{fN} \quad (11)$$

is a complex matrix only dependent on material parameters and the Matsubara frequency ω_l , which depends on T .

To obtain T_c , we apply the multimode method developed by Fominov *et al.* [11]. If we write down the components of the vector Eq. (10) and eliminate C , we obtain

$$\frac{dF_s(0)}{dx} = Q(\omega_l) F_s(0) \quad \text{with} \quad Q(\omega_l) = \frac{L_{21}(\omega_l)}{L_{11}(\omega_l)}, \quad (12)$$

which is analogous to Eq. (8) in [11]. From here, the problem is reduced to finding the highest T for which the determinant of a matrix \mathbf{K} is zero. If we include M modes ($m = 1, 2, \dots, M$) in addition to the single-mode method and take the first $M + 1$ Matsubara frequencies ($l = 0, 1, \dots, M$), the elements of \mathbf{K} are

$$K_{l0} = \frac{R(\omega_l) \cos(k_0 d_s) - k_0 \sin(k_0 d_s)}{\hbar(\omega_l + k_0^2 D_s/2)} \quad \text{and} \quad (13)$$

$$K_{lm} = \frac{R(\omega_l) \cosh(k_m d_s) + k_m \sinh(k_m d_s)}{\hbar(\omega_l - k_m^2 D_s/2)}, \quad (14)$$

where $R(\omega_l)$ is given by

$$R(\omega_l) = \text{Re}(Q(\omega_l)) + \frac{[\text{Im}(Q(\omega_l))]^2}{\text{Re}(Q(\omega_l)) + k_s \tanh(k_s d_s)} \quad (15)$$

in the function of $Q(\omega_l)$ and $k_s = \sqrt{2\omega_l/D_s}$. The quantities k_0 and k_m ($m = 1, 2, \dots, M$) are the smallest positive roots of

$$\ln\left(\frac{T_0}{T}\right) = \psi\left(\frac{1}{2} + \frac{\hbar k_0^2 D_s}{4\pi k_B T}\right) - \psi\left(\frac{1}{2}\right) \quad \text{and} \quad (16)$$

$$\ln\left(\frac{T_0}{T}\right) = \psi\left(\frac{1}{2} - \frac{\hbar k_m^2 D_s}{4\pi k_B T}\right) - \psi\left(\frac{1}{2}\right), \quad (17)$$

which are obtained from the self-consistency Eq. (4) and contain the digamma function ψ .

Using this method, we determine T_c numerically; the calculation is repeated with various values of T , for $0 < T < T_0$. By obtaining the roots k_0 and k_m of Eqs. (16) and (17), and evaluating $R(\omega_l)$ through Eq. (15), the matrix \mathbf{K} can be found for all T . The largest value of T for which $\det(\mathbf{K}) = 0$ corresponds to T_c . The multimode method with $M \rightarrow \infty$ is exact but in most cases the inclusion of $M = 8$ modes suffices.

To apply this numerical method with the minimum number of adjustable parameters, we have measured σ for Nb, Fe and Cr thin films for $T < 10$ K to be 1.9×10^6 (Ωm)⁻¹, 6.6×10^6 (Ωm)⁻¹, and 2.2×10^6 (Ωm)⁻¹, respectively. From these values, we estimate the electron mean free paths of Fe and Cr via $\ell = \sigma m v_F (n e^2)^{-1}$ with v_F the Fermi velocity; v_F for Fe [12] and Nb [13] is taken from literature, while for Cr we assume a similar v_F to Fe. The density number of electrons is $n = (8\pi/3) \cdot (m v_F / h)^3$ with m the electron mass, giving an ℓ of 2.7 nm and 0.9 nm for Fe and Cr, respectively. For Nb, we determine ℓ by choosing a value that gives the best fit (2.2 nm). With ℓ known, we calculate D for Nb, Fe, and Cr via $D = \ell v_F / 3$, giving 2.2×10^{-4} m²s⁻¹ for Nb, 18×10^{-4} m²s⁻¹ for Fe, and 6.0×10^{-4} m²s⁻¹ for Cr. Finally, we estimate the coherence lengths of Nb and Cr with $\xi_{s,n} = \sqrt{\hbar D_{s,n} / 2\pi k_B T_0}$, giving 5.8 nm for Nb (similar to [14]) and 9.6 nm for Cr, while for Fe $\xi_f = \sqrt{\hbar D_f / I}$, giving 3.7 nm (similar to [10]) assuming $I \sim 1000$ K [15]. For both Nb and Fe, $\xi > \ell$, which is indicative of dirty limit behavior and, therefore, justifies our use of the linearized Usadel equations. For the interfacial resistances we take $R_{Fe,Nb} \sim$

$10^{-15} \Omega m^2$ and $R_{Fe,Cr} \sim 10^{-17} \Omega m^2$ (the quality of the fit does not depend strongly on these parameters). The important material parameters used/calculated here are listed in Table I. With these values, the numerical model agrees well with the experimental data; see Fig. 3.

We have generalized the model to consider the behavior when the Fe layers are non-collinear; we use the linearized Usadel equations containing both the singlet and triplet components of the anomalous Green function [16]. We find that with a small change in 2θ , the angle between the polarizations of adjacent Fe layers, the T_c is more strongly reduced and the parity dependent oscillations fade away faster; see Fig. 3(a,i). In the limiting case of $2\theta = \pi$ we recover the SAF behavior. An applied magnetic field will produce a non-collinear configuration; however, in our samples this could not be achieved without directly suppressing the Nb T_c . With improved control of J the field required to reorient the layers could be substantially reduced.

In conjunction with the experimental results, this demonstrates that a large change in T_c can be obtained by switching the SAF between P and AP configurations. In the particular case of $N = 2$, which corresponds to the Oh *et al.* [9] spin valve, the change in T_c from AP to P is > 1 K, which is a many times higher than the changes experimentally observed in the analogous superconductor PSV structures [8].

This Letter has shown that the parity of AFs with perfect order have a profound effect on the proximity effect as predicted by Andersen *et al.* and that the results can be well described by the adaptation of the linearized Usadel equations to this new situation. However, there are important aspects of the results which are not explained on this basis. Firstly, there appears to be a longer period oscillation in T_c , which is visible in both data sets as an upturn in the trend in T_c for $N > 5$. Perhaps, more significantly, there appears to be a parity-dependence of the resistive transition width (ΔT_c) as shown in Fig. 3(c), which suggests that the nature of the superconducting transition is being affected.

	ξ	v_F	I	σ	D	ℓ
	nm	$\times 10^6 \text{ ms}^{-1}$	K	$\times 10^6 (\Omega m)^{-1}$	$\times 10^{-4} \text{ m}^2 \text{ s}^{-1}$	nm
Nb	5.8	0.3	...	1.9	2.2	2.2
Fe	3.7	2.0	1000	6.6	18	2.7
Cr	9.6	2.0	...	2.2	6.0	0.9

TABLE I: Important parameters used/*calculated* in this letter.

This work was supported by EPSRC UK. We thank Professor James Annett for theoretical discussions.

-
- [1] For reviews: A. I. Buzdin, Rev. Mod. Phys. **77**, 935 (2005); F. S. Bergeret, A. F. Volkov, and K. B. Efetov, Rev. Mod. Phys. **77**, 1321 (2005).
 - [2] J. S. Jiang *et al.*, Phys. Rev. Lett. **74**, 314 (1995).
 - [3] Brian M. Andersen *et al.*, Phys. Rev. Lett. **96**, 117005 (2006).
 - [4] C. Bell *et al.*, Phys. Rev. B **68**, 144517 (2003); Y. Cheng and M.B. Stearns, J. Appl. Phys. **67**, 5038 (1990).
 - [5] S. S. P. Parkin *et al.*, Phys. Rev. Lett. **64**, 2304 (1990).
 - [6] P. Koorevaar *et al.*, Phys. Rev. B **49**, 441 (1994); T. Mühge *et al.*, Phys. Rev. Lett. **77**, 1857 (1996); M. Vélez *et al.*, Phys. Rev. B **59**, 14659 (1999).
 - [7] P. G. de Gennes, Phys. Lett. **23**, 10 (1966); L. R. Tagirov, Phys. Rev. Lett. **83**, 2058 (1999); A. I. Buzdin *et al.*, Europhys. Lett. **48**, 686 (1999).
 - [8] Ion C. Moraru *et al.*, Phys. Rev. Lett. **96**, 037004 (2006); J. Y. Gu *et al.*, Phys. Rev. Lett. **89**, 267001 (2002); A. Potenza and C. H. Marrows, Phys. Rev. B **71**, 180503(R) (2005).
 - [9] Sangjun Oh *et al.*, Appl. Phys. Lett. **71**, 2376 (1997).
 - [10] J. W. A. Robinson *et al.*, Phys. Rev. B **76**, 094522 (2007).
 - [11] Ya. V. Fominov *et al.*, Phys. Rev. B **66**, 014507 (2002).
 - [12] M. K. Covo *et al.*, Phys. Rev. ST Accel. Beams **9**, 063201 (2006).
 - [13] D. K. Finnemore *et al.*, Phys. Rev. **149**, 231 - 243 (1966).
 - [14] A. S. Sidorenko *et al.*, Ann. Phys. (Berlin) **12**, 37 (2003).
 - [15] C. Kittel, *Introduction to Solid State Physics* (John Wiley & Sons, Inc., New York, 1956).
 - [16] M. Houzet and A. I. Buzdin, Phys. Rev. B **76**, 060504(R) (2007).